Extended Wind Stress Analyses for ENSO

ANDREW T. WITTENBERG

Atmospheric and Oceanic Sciences Program, Princeton University, Princeton, New Jersey

(Manuscript received 30 December 2002, in final form 21 August 2003)

ABSTRACT

Surface wind stresses are fundamental to understanding El Niño, yet most observational stress products are too short to permit multidecadal ENSO studies. Two exceptions are the Florida State University subjective analysis (FSU1) and the NCEP–NCAR reanalysis (NCEP1), which are widely used in climate research. Here, the focus is on the aspects of the stress most relevant to ENSO—namely, the climatological background, anomaly spectrum, response to SST changes, subannual ''noise'' forcing, and seasonal phase locking—and how these differ between FSU1 and NCEP1 over the tropical Pacific for 1961–99.

The NCEP1 stress climatology is distinguished from FSU1 by weaker equatorial easterlies, stronger off-equatorial cyclonic curl, stronger southerlies along the Peruvian coast, and weaker convergence zones with weaker seasonality. Compared to FSU1, the NCEP1 zonal stress anomalies (τ_x') are weaker, less noisy, and show less persistent westerly peaks during El Niño events. NCEP1 also shows a more stationary spectrum that more closely resembles that of equatorial east Pacific SST anomalies. After the 1970s, the equatorial trade winds and stress variability shift east and strengthen in FSU1, while the opposite occurs in NCEP1. Both products show increased mean convergence in the equatorial far west Pacific in recent decades, with weaker mean easterlies near the date line, an increased stress response to SST anomalies, and stronger interannual and subannual τ_x' in the central equatorial Pacific (Niño-4; 5°N–5°S, 160°E–150°W). The variance of Niño-4 τ_x' is highly seasonal in both datasets, with an interannual peak in October–November and a subannual peak in November–February; yet apart from interannual Niño-4 τ_x' after 1980, stress anomalies are not well correlated between the products. Newer and more reliable stress estimates generally fall between NCEP1 and FSU1, with most closer to FSU1.

1. Introduction

Although the wind stress over the sea surface is critical to ocean modeling and El Niño–Southern Oscillation (ENSO) forecasting, the true stress remains poorly known over most of the World Ocean for the past four decades. Historical stress analyses are largely based on wind velocities estimated from surface wave heights or measured by anemometers far from the surface. Such observations are prone to errors—like inaccurate conversions from Beaufort scale to wind speed and incorrect assumptions of anemometer heights (Cardone et al. 1990; Morrissey 1990; Isemer and Hasse 1991; Kent and Taylor 1997; Kent et al. 1999). Sparse measurements and an evolving observing system further give rise to aliasing and spurious trends (Wright and Thompson 1983; Clarke and Lebedev 1996, 1997; Kistler et al. 2001; Sterl 2001; Trenberth et al. 2001). Even given accurate pseudostresses at a known height, determining the surface stresses requires additional parameters not always measured at sea: surface currents and roughness, vertical wind shear, and the shape and motion of the observing platform (Smith 1988; Cardone et al. 1990; da Silva et al. 1994; Fairall et al. 1996, 2003; Yelland et al. 1998; Taylor et al. 1999; Kelly et al. 2001; Brunke et al. 2003).

To reduce these uncertainties one may impose constraints, such as dynamical balance (Zebiak 1990; Stevens et al. 2002), consistency with observed SST and sea level pressure (Ward 1992; Ward and Hoskins 1996; Clarke and Lebedev 1996, 1997; Patoux et al. 2003), and accuracy of the forced oceanic response (Graham 1994; Kirtman and Schneider 1996; Bonekamp et al. 2001; Hackert et al. 2001; Stammer et al. 2002; Wu and Xie 2003). Often the goal is a gridded wind stress analysis, which can then be used by climate researchers for model validation, data assimilation, and forecast initialization.

Numerous studies have described and compared tropical Pacific wind stress analyses over various time periods (see Jones and Toba 2001; Wittenberg 2002). Some have focused on the annual mean and seasonal cycle (McPhaden et al. 1988; Busalacchi et al. 1990; Landsteiner et al. 1990; Trenberth et al. 1990; Yang et al. 1997; Saji and Goswami 1997; Josey et al. 2002), others on departures from the annual cycle and decadal changes (Reynolds et al. 1989; Busalacchi et al. 1990; Graham 1994; Kleeman et al. 2001; Yang et al. 2001;

Corresponding author address: Dr. Andrew T. Wittenberg, Atmospheric and Oceanic Sciences Program, Princeton University, Princeton, NJ 08544-0710.
E-mail: atw@gfdl.noaa.gov

Wu and Xie 2003). Further work has aimed at validating satellite wind products (Atlas et al. 1993, 1996; Busalacchi et al. 1993; Liu et al. 1993; Bentamy et al. 1996, 1999, 2003; Grima et al. 1999; Kelly et al. 1999; Yu and Moore 2000; Meissner et al. 2001; Quilfen et al. 2001; Zhang and Gottschalck 2002). It has become clear that there are large differences among stress analyses, which produce substantial differences in forced ocean simulations (Latif 1987; Harrison et al. 1989; Busalacchi et al. 1990; Gordon and Corry 1991; Rienecker et al. 1996; Milliff et al. 1999; Auad et al. 2001; Huang 2001) and coupled ENSO simulations and forecasts (Chen et al. 1999; Kug et al. 2001; Harrison et al. 2002; Chen 2003).

Two analyses in particular have attracted attention from ENSO researchers: the Florida State University research-quality subjective pseudostress (FSU1; Stricherz et al. 1997) and the National Centers for Environmental Prediction–National Center for Atmospheric Research (NCEP–NCAR) reanalysis (NCEP1; Kalnay et al. 1996; Kistler et al. 2001). Each covers a long period (1961–99 for FSU1, 1948–present for NCEP1) as necessary for robust estimates of interannual-to-decadal variability; each has been widely used in climate studies, for example, to drive ocean simulations and analyses, generate initial conditions for ENSO forecasts, and fit statistical atmospheric models (Chen et al. 1995; Dewitte and Perigaud 1996; Behringer et al. 1998; Ji et al. 1998; Chen et al. 2000; Kleeman et al. 2001; Kug et al. 2001; Kang and Kug 2002; Kirtman et al. 2002; Tang 2002; Wittenberg 2002; Moore et al. 2003).

Despite anecdotal evidence that NCEP1 and FSU1 differ, there have been few systematic attempts to document how these differences might matter for ENSO. Auad et al. (2001) examined cross statistics of the NCEP1 and FSU1 stress anomalies. They found the NCEP1 anomalies to be substantially weaker along the equator and poorly correlated with FSU1 in the equatorial Pacific, east Pacific, and for intraseasonal variations. Others have confirmed that NCEP1 underestimates the stresses derived from buoys and high-quality ship observations (Shinoda et al. 1999; Smith et al. 2001). Chen (2003) found the FSU1 stresses to be much noisier than NCEP1, with better agreement between the products during warm events than cold events.[1] Efforts to merge these extended analyses and quantify their uncertainty have just begun (Putman et al. 2000; Smith et al. 2001; Taylor 2001). Meanwhile, questions remain regarding the relevance of the many existing climate studies based on FSU1 and NCEP1, and current researchers interested in the behavior of ENSO prior to the late 1970s must somehow decide how to utilize these products.

To ease this burden, this article will 1) document the FSU1/NCEP1 similarities and differences relevant to ENSO, namely the tropical Pacific climatological background, anomaly spectrum and response to SST changes, subannual ''noise'' forcing, and seasonal phase locking, and 2) show how these characteristics have changed over the past four decades.

2. Data

We consider monthly mean wind stresses computed using the highest resolution wind data available. NCEP1 provides a monthly mean stress $\boldsymbol{\tau}$, while FSU1 provides a binned monthly mean pseudostress $\langle \|\mathbf{u}_{10}\|\mathbf{u}_{10}\rangle$, where $\mathbf{u}_{10}$ is the vector wind 10 m above the sea surface, and angle brackets denote a monthly mean.[2] The FSU1 pseudostress is converted to stress using

$$\boldsymbol{\tau} = \rho_a c_d \langle \|\mathbf{u}_{10}\|\mathbf{u}_{10}\rangle \quad (1)$$

with air density $\rho_a = 1.2$ kg m^{-3} and drag coefficient $c_d = 1.3 \times 10^{-3}$.

Figure 1 shows running annual means of the zonal stress (τ_x) from these and other analyses, averaged over the ENSO-active Niño-4 region (5°S–5°N, 160°E–150°W). The FSU time series are similar to the University of Wisconsin–Milwaukee/Comprehensive Ocean–Atmosphere Dataset (UWM/COADS)[3] since they are based heavily on COADS after 1966. NCEP1 gives the weakest equatorial stresses of all products—for both the climatological trades and their interannual variations—and agrees poorly even with the NCEP–Department of Energy (DOE) Atmospheric Model Intercomparison Project II (AMIP-II) reanalysis (NCEP2). FSU1, on the other hand, agrees well both with FSU2 and with high-quality estimates from the variational analysis method Special Sensor Microwave Imager (VAM-SSM/I) and the National Aeronautics and Space Administration's Quick Scatterometer (QuikSCAT) data available for recent decades. The new European Centre for Medium-Range Weather Forecasts 40-year Re-Analysis (ERA40; a model-based reanalysis like the NCEP products) lies between FSU1 and NCEP1, and is generally closer to FSU1 except during the cold events of the latter 1990s.

The rest of this article will focus on FSU1 and NCEP1, as these are the end-members in Fig. 1 and are the products most widely used for extended ENSO studies. Monthly mean SSTs from the Smith et al. (1996) reconstruction are also examined. The data are averaged into 2° latitude by 5.625° longitude boxes covering the tropical Pacific Ocean (20°S–20°N, 129.375°E–84.375°W). A 12-month climatology is computed sep-

[1] Chen (2003) identified persistent westerly stress anomalies in FSU1 after 1998, which appear to have come from the ''quick look'' extension of his dataset (S. R. Smith 2001, personal communication). This feature is not present in the updated FSU1 product used here.

[2] NCEP1 incorrectly assimilated some Australian surface pressure estimates [paid observations (PAOBs)], but this error had little or no effect on tropical Pacific surface stresses (Kistler et al. 2001).

[3] Harrison and Larkin (1998) and Wu and Xie (2003) discuss climatological and ENSO aspects of COADS.

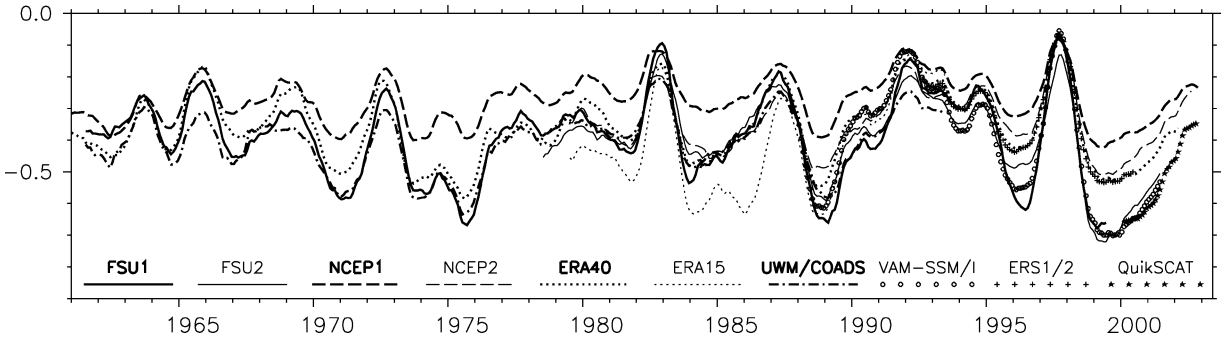

FIG. 1. Running annual means of ''observed'' zonal wind stress averaged over the Niño-4 region (5°S–5°N, 160°E–150°W). Data are from the FSU subjective analysis (FSU1, Stricherz et al. 1997); FSU objective analysis (FSU2, Bourassa et al. 2001); NCEP–NCAR reanalysis (NCEP1, Kistler et al. 2001); NCEP–DOE AMIP-II reanalysis (NCEP2); ECMWF 40-year reanalysis (ERA40; Simmons and Gibson 2000); ECMWF 15-year Re-Analysis (ERA-15; Gibson et al. 1999); UWM/COADS (da Silva et al. 1994); SSM/I VAM level 3.0 (VAM-SSM/I; Atlas et al. 1996); *European Remote Sensing Satellites 1/2* (*ERS1/2*) merged level 3.0 (*ERS1/2*, Quilfen et al. 2001); and SeaWinds/QuikSCAT level 3.0 (QuikSCAT; IFREMER/CERSAT 2002). The FSU pseudostresses and VAM-SSM/I 6-hourly winds are converted to surface stresses using (1).

arately for 1961–79 and 1980–99, and subtracted from the total fields to give monthly mean stress anomalies ($\boldsymbol{\tau}'$) and SST anomalies (SSTAs) for each dataset and period.

3. Climatology

a. Annual mean

Annual-mean climatologies of the wind stress and SST are shown in Fig. 2. The mean zonal stress ($\overline{\tau}_x$; Fig. 2a) is easterly except in the far eastern and western equatorial Pacific, and is important for maintaining the thermocline tilt and upwelling at the equator. The trade easterlies have a saddle shape with peaks in the central basin 12°–15° from the equator, weakening toward the coasts. Strong meridional gradients of $\overline{\tau}_x$ produce cyclonic curl and poleward Sverdrup transport over most of the tropical Pacific. NCEP1 has a more pronounced saddle than FSU1, with weaker equatorial easterlies and stronger cyclonic curl. Between 1961–79 and 1980–99, both products show weakening mean easterlies near the equatorial date line, strengthening easterlies in the southwest, and greater cyclonic curl. But, while FSU1 suggests the trades strengthened and shifted eastward, NCEP1 suggests they weakened and shifted westward.

Figure 2b shows the mean meridional stress $\overline{\tau}_y$, which is important for generating the south equatorial upwelling that contributes to the meridional asymmetry of the cold tongue. In the east Pacific, southerlies cross the equator and meet opposing northerlies in the intertropical convergence zone (ITCZ) between 5° and 12°N. In the central basin, weak northerlies cross the equator and meet opposing southerlies in the South Pacific convergence zone (SPCZ) between 5° and 17°S. The weakness of the NCEP1 ITCZ/SPCZ is well known (Janowiak et al. 1998; Pegion et al. 2000; Putman et al. 2000; Wu and Xie 2003). NCEP1 shows stronger southerlies than FSU1 in the southeast, but weaker southerlies crossing the equator in the central and eastern Pacific. Hence in the east NCEP1 shows less divergence than FSU1 at the equator and has a ''double ITCZ'' near 5°S that is much stronger than in FSU1. After 1980 both products show increased southerlies in the southwest and greater convergence in the western equatorial Pacific. But, while FSU1 shows stronger southerlies along the southeast coast and weaker mean divergence in the equatorial eastern Pacific, NCEP1 shows just the opposite.

The SST climatology (Fig. 2c) consists of a cold tongue that extends up the coast of South America and westward along the equator, and a vast warm pool in the west connected by a band of >27°C water to a smaller warm pool south of Mexico. Between 1961–79 and 1980–99, the SST data suggest a warming and eastward expansion of the western warm pool, a widening of the warm band, a weaker cold tongue, and a reduced zonal SST contrast across the basin. To the extent that the trade wind stress is governed by hydrostatic sea level pressure (SLP) changes within the planetary boundary layer (PBL) induced by local SST gradients (Lindzen and Nigam 1987), the east Pacific warming would appear consistent with the weakening trades in NCEP1. But SLP is also controlled by free tropospheric temperatures (Wang and Li 1993; Chiang et al. 2001); if these are most sensitive to SST changes in the west Pacific where there is strong moisture convergence and warm SST, then the warming and eastward expansion of the warm pool would appear consistent with the strengthening and eastward shift of the trades in FSU1. Warmer SSTs also destabilize the PBL in the east, mixing momentum downward and increasing the surface stress (Hayes et al. 1989; Wallace et al. 1989; Liu et al. 2000; Chelton et al. 2001; Hashizume et al. 2002). Unlike NCEP1, FSU1 shows increased surface wind convergence in the equatorial central Pacific, consistent with observed decreases in SLP and outgoing longwave radiation and observed increases in SST, specific humidity, and rainfall (Wu and Xie 2003).

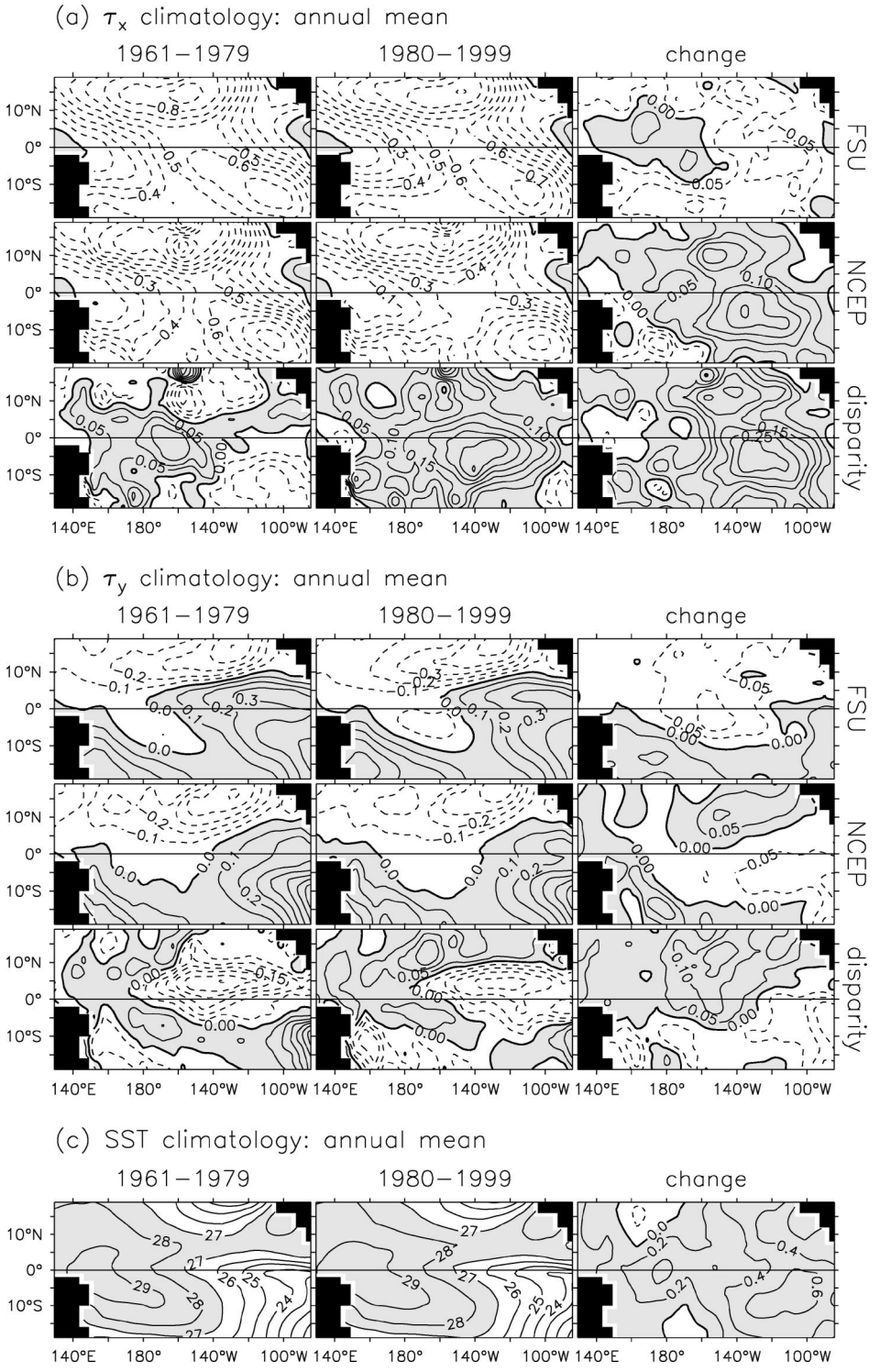

FIG. 2. Annual-mean climatology of (a) zonal and (b) meridional wind stress (dPa), and (c) SST (°C). Fields are shown for 1961–79 (first column) and 1980–99 (second column). The change from the former period to the latter is shown in the third column. Rows correspond to FSU1 (first row), NCEP1 (second row), and their difference (NCEP1 minus FSU1, third row).

b. Seasonal cycle

Compared to NCEP1, FSU1 generally shows much stronger seasonality of $\overline{\tau}_y$ and divergence due to its more intense ITCZ (not shown). Between 1961–79 and 1980–99, both products show stronger monsoons in the southwest, weaker $\overline{\tau}_x$ variations in the southeast, and a greater tendency toward an annual cycle in the west instead of a semiannual cycle. Both products also show greater seasonality of the stress divergence in the central equatorial Pacific and less seasonality near the ITCZ. For other aspects of the seasonal cycle, FSU1 and NCEP1 give conflicting changes after 1980. FSU1 shows increased seasonality of the central Pacific easterlies and east Pacific cross-equatorial southerlies, while NCEP1 shows the opposite. FSU1 shows increased seasonal curl variations near the equator, while NCEP1 shows a broad decrease across the east Pacific. The SST data indicate some enhanced May warming in the east and a slightly *stronger* semiannual cycle in the west, but otherwise there is little change in the annual cycle of SST at the equator.

4. Anomaly patterns

a. Interannual variability

ENSO behavior is highly sensitive to changes in the wind stress response to SSTAs (Neelin 1990; Kirtman 1997; An and Wang 2000; Cassou and Perigaud 2000). Zonal stress anomalies alter the slope of the thermocline, the strength of equatorial upwelling, and the zonal currents that advect the edge of the warm pool—each of which affects equatorial SST. Variations in τ_y' likewise affect upwelling and biological production just south of the equator and near the coast of South America. Changes in stress curl generate equatorial Rossby waves, which discharge heat from the equatorial band and terminate El Niño; changes in wind convergence affect convection, altering the surface heat balance and the atmospheric sensitivity to SST.

For simplicity we shall consider only the linear part of the stress response to SST anomalies.[4] Interannual SSTAs are concentrated in the cold tongue and are strongly correlated with SSTAs averaged over the Niño-3 region (5°S–5°N, 150°–90°W). Figure 3 shows regressions of $\boldsymbol{\tau}$ onto Niño-3 SSTA. Both FSU1 and NCEP1 give equatorial westerlies and off-equatorial easterlies in the west-central basin, weak easterlies near the eastern boundary, northerlies spanning the northern tropical Pacific, and southerlies across the southwest and equatorial southeast Pacific. There is cyclonic stress curl on both sides of the equator in the central Pacific, convergence along the equator, and divergence in the off-equatorial eastern Pacific. The meridional center of the τ_x' response lies a degree or two south of the equator, and the northern cyclone center (~5°N) is closer to the equator than the southern cyclone center (~10°S).

Between 1961–79 and 1980–99, the FSU1 and NCEP1 τ_x' responses to Niño-3 SSTA (Fig. 3a) show some similar changes at the equator, including stronger westerly anomalies near the date line, stronger easterly anomalies near the western boundary, and weaker easterly anomalies near the eastern boundary. But there are also striking differences between the analyses. For 1961–79, the equatorial westerlies (and associated off-equatorial cyclonic curl) in the two products have similar amplitudes, but in FSU1 the response is centered near 175°W, while in NCEP1 it is focused near 145°W with only a weak tail extending past the date line. For 1980–99, the two products are in better agreement regarding the position of the westerly peak near 165°W, but in NCEP1 the response is less than 60% as strong as in FSU1. Thus, while FSU1 indicates that the westerly response to Niño-3 SSTA strengthened and spread eastward after 1980, NCEP1 shows just the opposite.

The meridional stress response (Fig. 3b) also differs substantially between FSU1 and NCEP1. Although the NCEP1 response better resembles FSU1 during 1980–99, for both periods NCEP1 shows weaker southerly stress anomalies in the SPCZ region and equatorial eastern Pacific and much weaker meridional convergence anomalies than FSU1 in the vicinity of the ITCZ. Between 1961–79 and 1980–99, the interannual variability of τ_y' increases along the equator in both datasets, especially FSU1 which shows a change toward a more northerly wind stress response near 140°W. NCEP1 shows a smaller such change occurring 20°–30° farther west. FSU1 shows a decrease in interannual convergence anomalies in the west and an increase in the east, while NCEP1 shows an *increase* in the west and a decrease off-equator in the central and eastern tropical Pacific. The weakening of interannual τ_y' between 5° and 10°S in NCEP1 is not as apparent in FSU1.

Figure 3c shows how SSTAs are related to the Niño-3 index. One must ask whether the very small decadal changes in the SSTA pattern can account for the rather large changes in *either* of the wind stress analyses, if indeed the stress changes are real. Between 1961–79 and 1980–99, the SSTA pattern shifted eastward by 5°–10° longitude, and the strength of the zonal SSTA gradients increased as did the interannual SSTA variance toward the coasts. These changes appear consistent with the eastward shift and strengthening of the stress response in FSU1, to the extent that the stress anomalies are driven by anomalous SST gradients. Changes in *mean* SST and wind convergence between 1961–79 and 1980–99 (Fig. 2c) may also have modified the stress response, since the atmospheric heating that drives the winds is a nonlinear function of the total SST and wind convergence (Kleeman 1991; Wang and Li 1993; Battisti et al. 1999; Cassou and Perigaud 2000).

[4] In reality the stress response is a function of season (Yang et al. 2001) and differs between warm and cold events (Kang and Kug 2002).

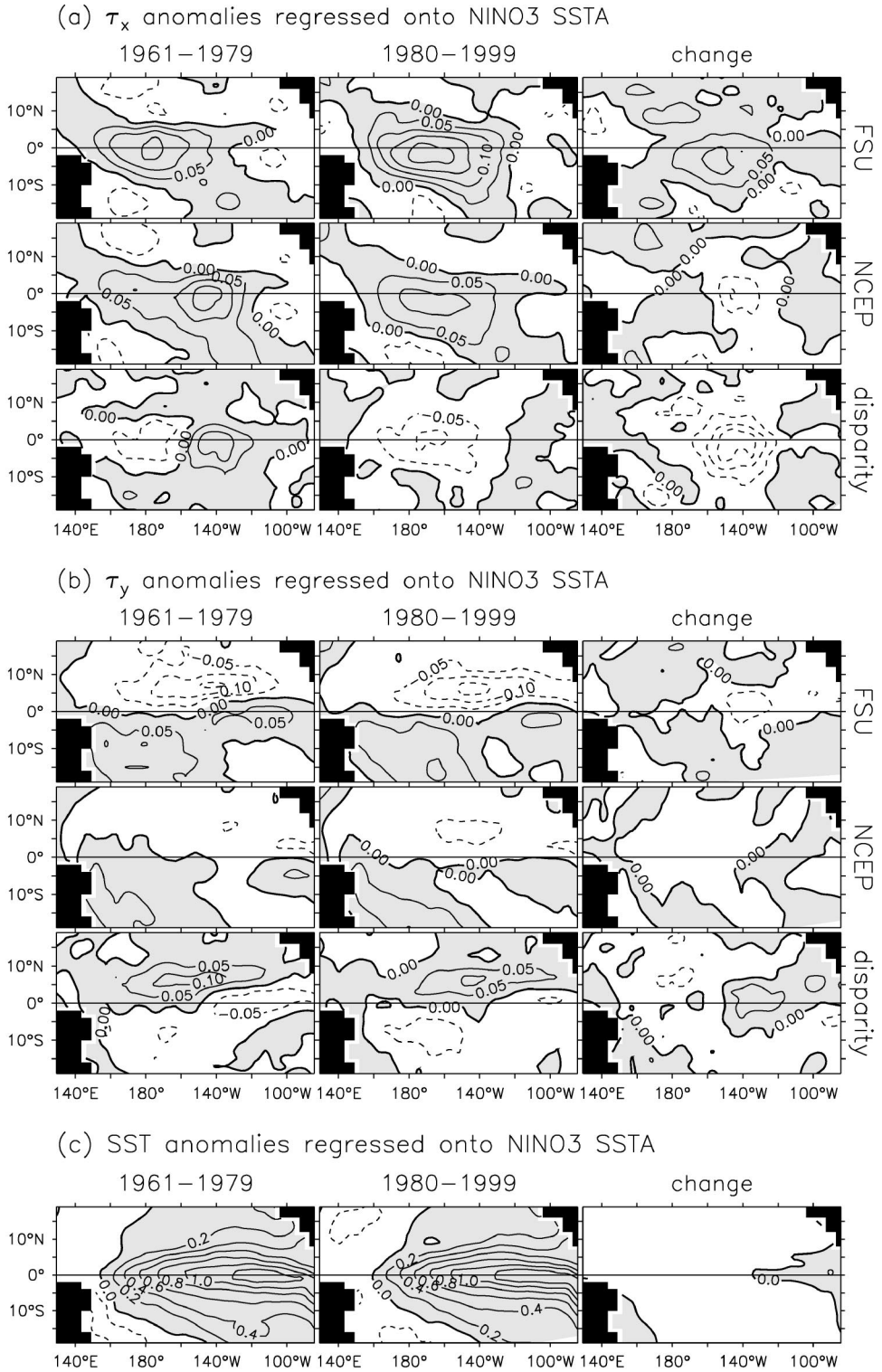

FIG. 3. As in Fig. 2 but for regressions of anomalies onto Niño-3-average SST anomalies. Units as in Fig. 2 but divided by °C.

b. Subannual variability

Many studies have suggested that intraseasonal variability can trigger and/or amplify ENSO events, though the relationship is not always robust (Zhang et al. 2001; Zhang and Gottschalck 2002). To extract these subannual signals, we first low-pass filter the monthly mean anomalies in each dataset via two applications of a 6-month running mean and then remove this low-pass signal from the original monthly mean anomalies.

Figure 4 shows the standard deviation of the subannual signal that remains. The subannual τ_x' is weak near the coasts, especially in the east, but away from the equator the subannual component is stronger than the interannual. At the equator, FSU1 gives a subannual τ_x' even stronger than the interannual, while NCEP1 shows much weaker subannual variability. Between 1961–79 and 1980–99, both FSU1 and NCEP1 show a strengthening of subannual τ_x' variance in the west Pacific and a weakening in the central Pacific around 5°–10°N. But in FSU1 the subannual variance in the east Pacific increases, while in NCEP1 it decreases.

For τ_y', the subannual variability is generally comparable to the interannual. Apart from a broad minimum near the equator, there is little agreement between FSU1 and NCEP1 regarding the structure of the subannual τ_y' variance. In particular, FSU1 has much stronger equatorial τ_y' variance than NCEP1. Between 1961–79 and 1980–99, both products give increased variance in the west, but FSU1 gives a much stronger increase in the east than NCEP1. The subannual curl and divergence anomalies (not shown) are also much stronger in FSU1 than NCEP1, especially near the equator. FSU1 shows increased curl and divergence variability in the far eastern and western equatorial Pacific and a decrease in variability over the central Pacific that is focused farther west than in NCEP1.

5. Anomaly time series

a. The time series

Standardized time series of Niño-4 τ_x' and Niño-3 SSTA are shown in Figs. 5a, 6a, and 7a, with the standard deviation scale σ and lag-1-month autocorrelation ϕ_1 indicated above each plot. Note that the standard deviation of FSU1 is nearly twice that of NCEP1. For both stress products, τ_x' is well correlated with SSTA (0.65 for FSU1, 0.74 for NCEP1). However, the Niño-3 SST anomalies ($\phi_1 = 0.91$) are more persistent in time than the Niño-4 zonal stress anomalies in either NCEP1 ($\phi_1 = 0.82$) or FSU1 ($\phi_1 = 0.72$).

Strikingly, the differences between the FSU1 and NCEP1 anomalies are nearly as large as the stress anomalies themselves. The correlation of FSU1 and NCEP1 with each other (0.80) is only slightly larger than their correlation with SSTA. The FSU1 stress anomalies are generally stronger, noisier, and have more persistent westerly peaks than NCEP1. Compared to NCEP1 or SSTA, FSU1 exhibits weaker interannual variability during the 1960s and 1970s and weaker El Niño anomalies in 1982–83 and 1997–98. The 1991–92 warm event, on the other hand, is stronger in FSU1 than in NCEP1 or SSTA, stronger even than the 1982–83 and 1997–98 events in FSU1. The 1996 cold event is also larger in FSU1 than in NCEP1 or SSTA.

A ''climate shift'' is apparent in all three time series around 1976–77. In NCEP1, part of the shift may be an artifact related to the introduction of satellite data (Santer et al. 1999; Kistler et al. 2001). However, the shift is evident in multiple fields throughout the Pacific ocean and atmosphere (Nitta and Yamada 1989; Trenberth 1990; Gaffen et al. 1991; Graham 1994; Trenberth and Hurrell 1994; Nitta and Kachi 1994; Wang 1995; Morrissey and Graham 1996; Kachi and Nitta 1997; Zhang et al. 1997; Garreaud and Battisti 1999; Krishnamurthy and Goswami 2000; Goswami and Thomas 2000; An and Wang 2000; Xie et al. 2000; Wu and Xie 2003). This suggests that it may well be real and possibly independent of ENSO (Latif et al. 1997; Wang and An 2002).

b. Spectra

Figures 5b, 6b, and 7b provide continuous wavelet transforms of the anomaly time series. Each wavelet diagram is like a musical score for the time series with the lower notes (longer periods) toward the bottom (Lau and Weng 1995). Such diagrams have proved convenient for examining interdecadal changes in ENSO (Gu and Philander 1995; Wang and Wang 1996; Torrence and Compo 1999; Torrence and Webster 1998, 1999). ENSO appears in all three figures as a concentration of variance between 1 and 8 yr. That most of the blobs of variance are not much wider than the cone of influence confirms that ENSO events often occur in isolation, separated by long periods of relative inactivity (Larkin and Harrison 2002; Kessler 2002). The spectral power near 2 yr waxes and wanes in roughly an 8-yr cycle, while the power at 4 yr strengthens every 15 yr or so. There is also a gradual increase in variance at periods longer than 4 yr.

Figures 5c, 6c, and 7c show time-averaged spectra for 1961–79 and 1980–99. There is more power at subannual time scales for τ_x' than for SSTA, especially at periods of 3 months or less where τ_x' shows more power than red noise. Both τ_x' and SSTA show broad peaks in the 1–8-yr band that become stronger after 1980. The spectral peaks at 12–15 yr are stronger in τ_x' than in SSTA, but the significance of these peaks is dubious as they cannot clearly be distinguished from red noise.

The spectra reveal many differences among the time series. The NCEP1 spectrum is more stationary in time than FSU1 and looks more similar to SSTA. In the 0–6-month band, FSU1 has relatively more power than NCEP1 and shows more of an increase in variance after 1980 than either NCEP1 or SSTA. In the 6–12-month

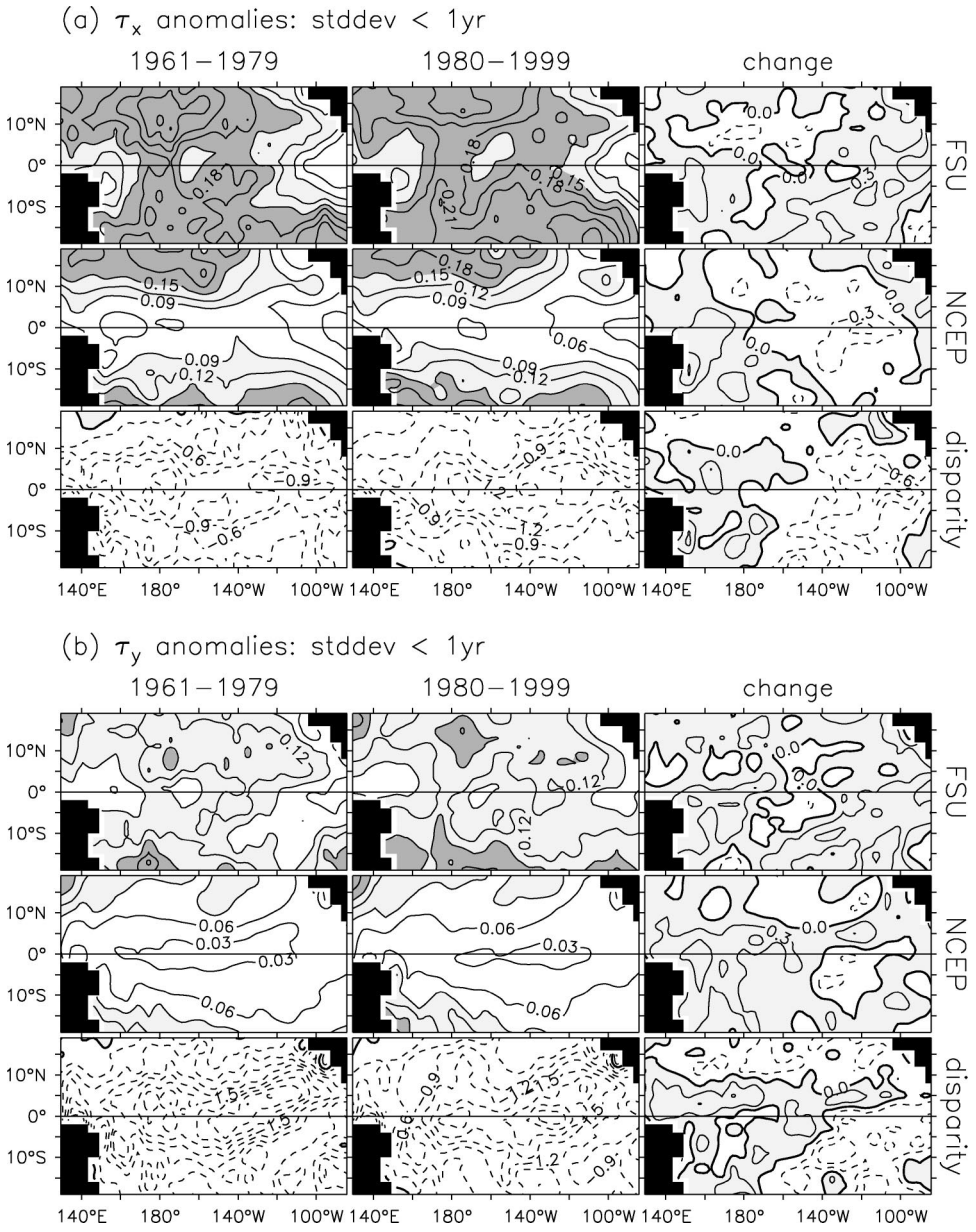

FIG. 4. Standard deviations of (a) zonal and (b) meridional wind stress anomalies (dPa) at periods less than 1 yr, for 1961–79 (first column) and 1980–99 (second column). The log-base-2 of the ratio of the latter period over the former is also shown (third column). Rows correspond to the FSU1 analysis (first row), the NCEP1 analysis (second row), and the log-base-2 of their ratio (NCEP1 over FSU1, third row).

band, FSU1 shows significantly *less* power than the red noise spectrum, while NCEP1 and SSTA cannot be clearly distinguished from red noise. In the interannual band, FSU1 shows a much stronger increase in variance between 1961–79 and 1980–99 than either NCEP1 or SSTA. FSU1 shows the greatest increase at 2.5 yr, at the short-period end of the active band, while in NCEP1 and SSTA the entire active band shifts toward *longer* periods with only a slight increase in amplitude.

Figures 5d, 6d, and 7d show the running variances in the 0–1-yr band and the 1–8-yr band. The interannual SSTA variance has gradually changed over the past four decades with quiet periods during the early 1960s, late 1970s, and early 1990s and active periods during the early 1970s, mid-1980s, and late 1990s. Most of these changes are mirrored in the τ_x' data, though neither stress product shows reduced interannual variance during the early 1990s when the decrease in variance at 4 yr is offset by an increase at 1–2 yr. The very strong El Niño of 1997–98 and its aftermath produce highly significant interannual variance peaks in all three datasets.

The NCEP1 τ_x' variance is more uniform in time than

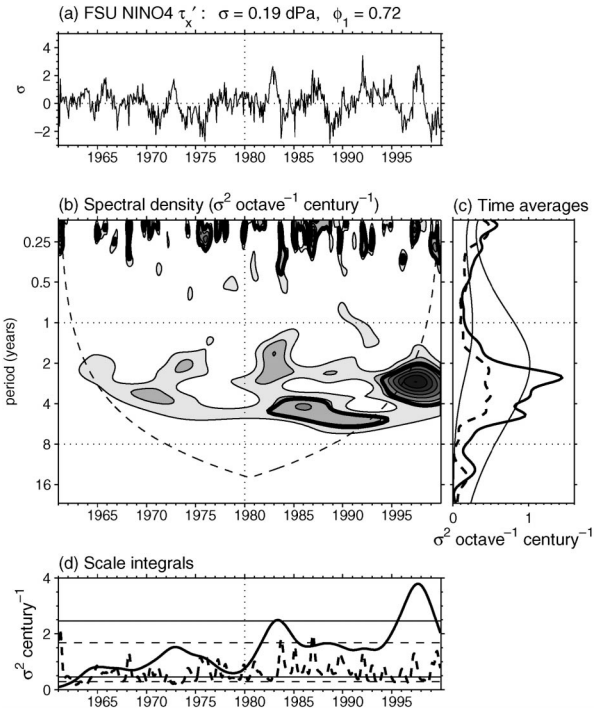

FIG. 5. (a) Time series of standardized monthly anomalies for the FSU1 zonal wind stress averaged over the Niño-4 region (5°S–5°N, 160°E–150°W). Anomalies are with respect to the 1961–99 climatology. The standard deviation σ and lag-1 autocorrelation ϕ_1 are indicated above the plot. (b) Spectral density of the time series, obtained by convolution with a Morlet wavenumber-6 wavelet. The base contour and contour interval are 0.5 σ^2 octave^{-1} century^{-1}. The dashed line (cone of influence) represents twice the *e*-folding time for the wavelet response to a spike in the time series; below this line the spectral density is underestimated due to edge effects. The thick contour encloses the 95th percentile for red noise realizations with the same σ and ϕ_1 as the time series. (c) Time-averaged spectra for 1961–79 (thick dashed) and 1980–99 (thick solid). Thin lines bracket the central 90% of wavelet spectra calculated from 20-yr realizations of the red noise. (d) Running variance in the 0–1-yr spectral band (thick dashed) and the 1–8-yr band (thick solid). Thin lines bracket the central 90% of running variances calculated from red noise.

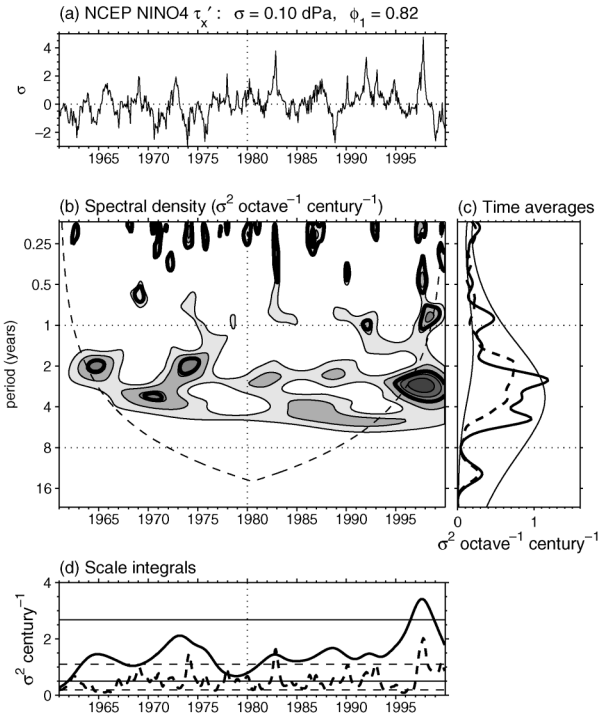

FIG. 6. As in Fig. 5 but for the NCEP1 zonal wind stress anomalies.

either FSU1 or SSTA. The FSU1 interannual variance increases strongly toward the latter half of the record, so the spectral variations of SSTA seem more consistent with NCEP1 than with FSU1. The stress products also show different changes in the 0–1-yr band: FSU1 shows heightened activity from 1983 to 1993, while NCEP1 shows fairly uniform noise activity apart from three prominent and isolated spikes in 1973–74, 1982–83, and 1997–98.

c. Seasonality of the anomaly variance

The annual cycles of Niño-4 τ_x' and Niño-3 SSTA variance are shown in Fig. 8. The standard deviation (σ) scales above each plot confirm that the stress anomalies (especially FSU1) have a larger subannual component than do the SST anomalies. Figure 8a shows that the anomaly variance changes through the calendar year.

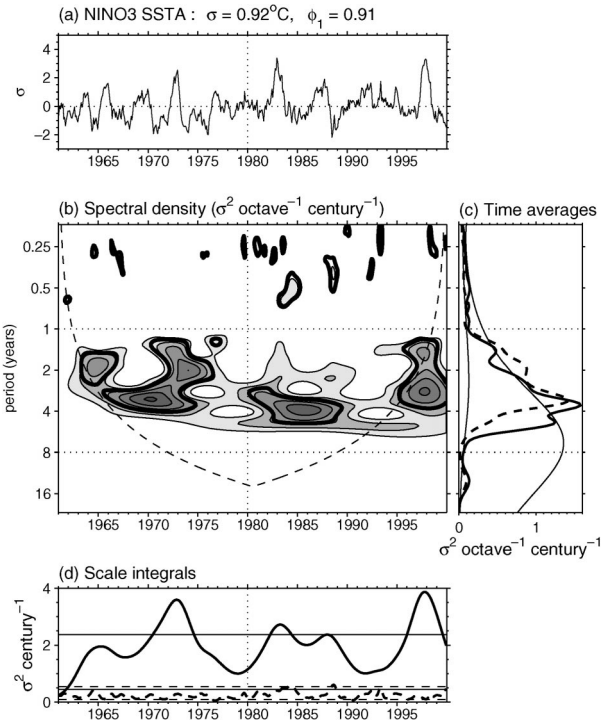

FIG. 7. As in Fig. 5 but for SST anomalies averaged over the Niño-3 region (5°S–5°N, 150°–90°W).

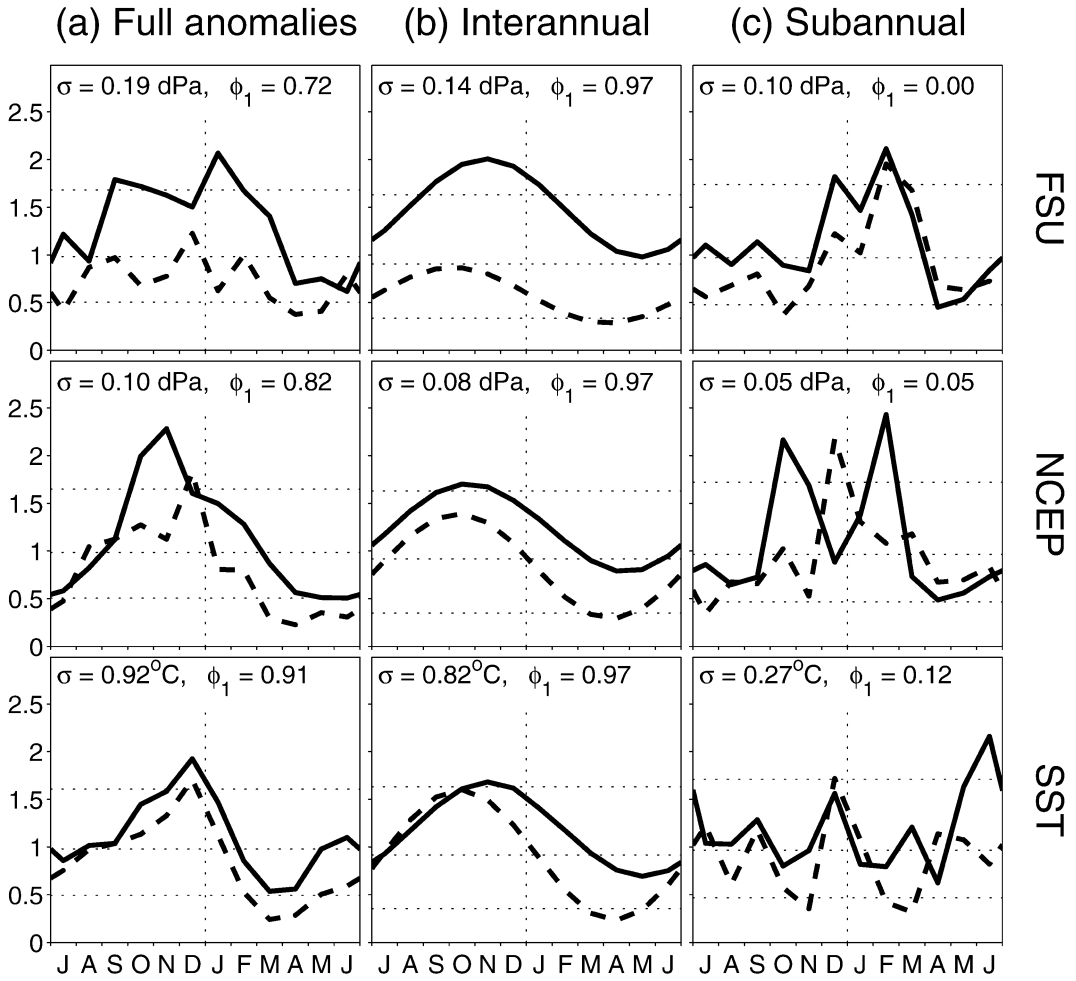

FIG. 8. Monthly variance of the anomalies for FSU1 and NCEP1 τ_x' averaged over Niño-4, and SSTA averaged over Niño-3. The anomalies have been filtered to retain (a) all periods, (b) periods greater than 1 yr, and (c) periods less than 1 yr. The variance is shown for 1961–79 (dashed) and 1980–99 (solid) and is in units of σ^2, where σ is the standard deviation over the entire 1961–99 period (labeled). The horizontal axis runs from Jul to Jun. Horizontal dotted lines give the median variance and 95% confidence band for 10 000 realizations of stationary red noise with the same σ and $\phi_1 \geq 0$ as the filtered 1961–99 time series.

The SSTA variance, for example, is 4 times stronger in December than in March. The τ_x' variance also tends to peak near the end of the calendar year, although FSU1 is not as strongly locked to the annual cycle as NCEP1. Between 1961–79 and 1980–99, there is little change in the cycle of SSTA variance apart from an overall strengthening. The wind stress products show more substantial changes, with both indicating an increased annual cycle of anomaly variance. However, in NCEP1 the December peak narrows and shifts to November, while in FSU1 the broad August–February peak shifts to September–March.

Figure 8b shows that the interannual variances of τ_x' and SSTA are clearly phaselocked to the annual cycle with anomalies most variable in boreal autumn and least variable in boreal spring. Between 1961–79 and 1980–99, all three datasets show a general strengthening of the variance and a shift of the cycle of variance so that it peaks slightly later in the year. But, while SSTA shows a weakening of the cycle of interannual variance, NCEP1 shows little change, and FSU1 actually shows a strengthening. The cycles in the three datasets are all in phase during 1961–79, but during 1980–99 NCEP1 is shifted a few weeks earlier than FSU1 and SSTA. In general, the calendar phasing of interannual anomalies appears robust with little dependence on dataset and little change between decades.

The seasonal cycle of subannual variance (Fig. 8c) is more complex. The subannual Niño-3 SSTA variance does not show much of a cycle, apart from a weak peak in December and a June peak during 1980–99. The subannual Niño-4 τ_x' variance, however, shows a strong cycle with decreased variance in late boreal spring and summer and increased variance in boreal winter. The subannual peaks during February–March occur at the time of year when the eastern equatorial Pacific is warm-

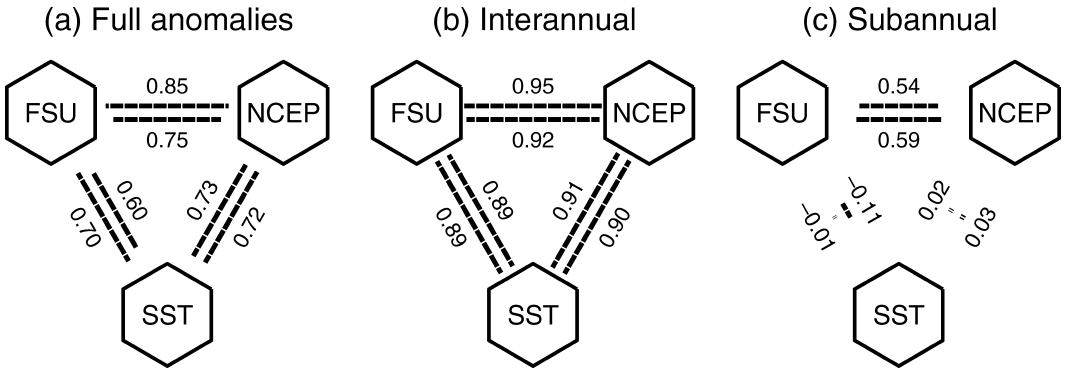

FIG. 9. Correlations among FSU1 and NCEP1 Niño-4 τ_x', and Niño-3 SSTA, represented graphically by the length of the links between variables. Inner links are for 1961–79, and outer links are for 1980–99. Correlations are shown for (a) the full anomalies, (b) anomalies filtered to retain only periods greater than 1 yr, and (c) anomalies filtered to retain only periods less than 1 yr.

est and convection is most active, while the October–December peaks stem from the skewness of ENSO τ_x' toward westerly events. Interestingly, the February peaks in subannual Niño-4 τ_x' variance have no analog in Niño-3 SSTA. Between 1961–79 and 1980–99, the subannual variance in FSU1 increased in every season except boreal spring, and the February peak in FSU1 broadened to include December and January. The December peak in NCEP1, on the other hand, split into two peaks: one in October–November and one in February. In general the calendar phasing of the subannual variability appears less robust than for ENSO.

d. Cross correlations

Cross correlations of Niño-4 τ_x' and Niño-3 SSTA are shown in Fig. 9. Hexagons represent the time series of Figs. 5a–7a, and connecting links indicate correlations between time series for 1961–79 (inner links) and 1980–99 (outer links). Clearly the interannual correlations (Fig. 9b) are the strongest, with the links between the stress and SST nearly as strong as those between the stress products. The subannual correlations (Fig. 9c) are much weaker: subannual τ_x' is linearly independent of large-scale SSTAs, and the subannual link between the stress analyses is tenuous. In general the SSTAs are better correlated with NCEP1 than with FSU1, especially prior to 1980.

The fractional changes in correlations between 1961–79 and 1980–99 are fairly small. There is little change in the links with SST, apart from an increased relationship between the full FSU1 and SST anomalies due to less negative subannual correlation. FSU1 and NCEP1 agree best for 1980–99, as evidenced by their increased correlation with each other (except for subannual time scales) and their more similar correlations with SSTAs.

6. Conclusions

Although NCEP1 and FSU1 are the most widely used wind stress products for extended ENSO studies, many researchers remain unaware of the large differences between them. To remedy this, we have compared the NCEP1 and FSU1 stresses for 1961–99, focusing on aspects relevant to ENSO.

The NCEP1 climatology is distinguished from FSU1 by weaker equatorial easterlies, stronger off-equatorial cyclonic curl, weaker cross-equatorial southerlies in the east Pacific, stronger southerlies along the Peruvian coast, and weaker convergence zones with weaker annual variations. Changes in the mean state between 1961–79 and 1980–99 differ as well: FSU1 indicates an eastward shift and strengthening of the equatorial trade winds, while NCEP1 suggests a westward shift and weakening of the trade winds. Changes in the annual cycle of wind stress also differ between the analyses, and appear unrelated to changes in the annual cycle of SST.

During El Niño, NCEP1 shows westerly stress anomalies that peak farther east than in FSU1. NCEP1 also exhibits a much weaker meridional stress response (owing to weaker convergence zones in that product) and lacks the cross-equatorial southerly anomalies evident in FSU1. Between 1961–79 and 1980–99, NCEP1 shows a weakening and westward spread of the zone of interannual τ_x' variability. FSU1, on the other hand, shows a strengthening and eastward spread consistent with increased SST variability in the east Pacific.

There is good temporal correlation of western equatorial Pacific (Niño-4) τ_x' between FSU1 and NCEP1 on interannual time scales. Small-scale anomalies, however, poorly correlated except for interannual anomalies in the western Pacific after 1980. Both interannual and subannual variability are stronger in FSU1 than NCEP1, notably for τ_x' near the date line and τ_y' near convergence zones. Stress anomalies are stronger and noisier in FSU1, but NCEP1 shows more extreme westerly peaks in the Niño-4 region during El Niño. Large event-to-event differences between the analyses are evident.

The spectrum of Niño-4 τ_x' in NCEP1 is more stationary in time than in FSU1 and appears to be more

consistent with Niño-3 SSTA especially before 1980. Compared with FSU1, NCEP1 shows a smaller fraction of the Niño-4 τ_x' variability occurring at time scales of 3 months or less. Between 1961–79 and 1980–99, the ENSO variability in FSU1 shifts toward shorter periods, while that in NCEP1 and SSTA shifts toward longer periods. The seasonal cycle of interannual variance becomes stronger in FSU1, but hardly changes in NCEP1. The seasonal cycle of subannual variance, and the decadal changes in that cycle, are also quite different between the analyses.

NCEP1 and FSU1 have come into better agreement since 1980, and many similarities are clear. At the equator between 1961–79 and 1980–99, both show increased mean convergence in the far western Pacific, a weakening of the mean easterlies near the date line, increased subannual and interannual variability in Niño-4, and a stronger τ_x' response to SST anomalies. The interannual variance of Niño-4 τ_x' peaks between October and November, the subannual variance between November and February. Niño-3 SST and Niño-4 τ_x' are strongly correlated on interannual time scales, but uncorrelated on subannual time scales. The following wind stress response to an ENSO warm event appears robust to dataset and time period: westerly anomalies peak in the west-central Pacific just south of the equator; easterly anomalies appear off-equator and in the east; cyclonic stress curl anomalies in the north lie closer to the equatorial waveguide than in the south; and the anomalous stress is generally equatorward, except in the southeastern part of the basin.

For extended ENSO studies over the tropical Pacific, at large spatial and temporal scales, FSU1 is recommended over NCEP1—it agrees better with independent observations and updated analyses, both for the tropical Pacific climatology and the anomaly response to SST changes. Historical wind stresses, however, will never be certain, and climate researchers must acknowledge this uncertainty when using stress analyses to drive ocean simulations, fit statistical stress models, and evaluate atmospheric general circulation models.

Acknowledgments. The support of the NASA Earth System Science Fellowship Program and NOAA/GFDL are gratefully acknowledged. A. Rosati, G. K. Vallis, and two anonymous reviewers provided helpful comments. S. R. Smith and FSU/COAPS supplied the FSU pseudostresses. The IRI/LDEO Climate Data Library and NOAA-CIRES Climate Diagnostics Center supplied the SST reconstruction and NCEP reanalyses. R. W. Reynolds, T. M. Smith, and D. C. Stokes provided insights into the SST data. Analysis tools were provided by C. Torrence and G. Compo at paos.colorado.edu/research/wavelets and NOAA/PMEL TMAP at ferret.wrc.noaa.gov. ERA obtained via www.ecmwf.int/research/era, UWM/COADS via ingrid.ideo.columbia.edu, VAM-SSM/I via dods.jpl.nasa.gov, ERS and QuikSCAT via www.ifremer.fr/cersat.

REFERENCES

An, S.-I., and B. Wang, 2000: Interdecadal change of the structure of the ENSO mode and its impact on the ENSO frequency. *J. Climate*, **13,** 2044–2055.

Atlas, R., R. N. Hoffman, and S. C. Bloom, 1993: Surface wind velocity over the oceans. *Atlas of Satellite Observations Related to Global Change*, R. J. Gurney, J. L. Foster, and C. L. Parkinson, Eds., Cambridge University Press, 129–139.

——, ——, ——, J. C. Jusem, and J. Ardizzone, 1996: A multiyear global surface wind velocity dataset using SSM/I wind observations. *Bull. Amer. Meteor. Soc.*, **77,** 869–882.

Auad, G., J. Miller, J. O. Roads, and D. Cayan, 2001: Pacific Ocean wind stress and surface heat flux anomalies from NCEP reanalysis and observations: Cross-statistics and ocean model responses. *J. Geophys. Res.*, **106,** 22 249–22 265.

Battisti, D. S., E. S. Sarachik, and A. C. Hirst, 1999: A consistent model for the large-scale steady surface atmospheric circulation in the Tropics. *J. Climate*, **12,** 2956–2964.

Behringer, D. W., M. Ji, and A. Leetmaa, 1998: An improved coupled model for ENSO prediction and implications for ocean initialization. Part I: The ocean data assimilation system. *Mon. Wea. Rev.*, **126,** 1013–1021.

Bentamy, A., Y. Quilfen, F. Gohin, N. Grima, M. Lenaour, and J. Servain, 1996: Determination and validation of average wind fields from ERS-1 scatterometer measurements. *Global Atmos. Ocean Syst.*, **4,** 1–29.

——, P. Queffeulou, Y. Quilfen, and K. Katsaros, 1999: Ocean surface wind fields estimated from satellite active and passive microwave instruments. *IEEE Trans. Geosci. Remote Sens.*, **37,** 2469–2486.

——, K. B. Katsaros, A. M. Mestas-Nuñez, W. M. Drennan, E. B. Forde, and H. Roquet, 2003: Satellite estimates of wind speed and latent heat flux over the global oceans. *J. Climate*, **16,** 637–656.

Bonekamp, H., G. J. van Oldenborgh, and G. Burgers, 2001: Variational assimilation of tropical atmosphere–ocean and expendable bathythermograph data in the Hamburg Ocean primitive equation ocean general circulation model, adjusting the surface fluxes in the tropical ocean. *J. Geophys. Res.*, **106,** 16 693–16 709.

Bourassa, M. A., S. R. Smith, and J. J. O'Brien, 2001: A new FSU winds and flux climatology. Preprints, *11th Conf. on Interactions of the Sea and Atmosphere*, San Diego, CA, Amer. Meteor. Soc., 9–12.

Brunke, M. A., C. W. Fairall, X. Zeng, L. Eymard, and J. A. Curry, 2003: Which bulk aerodynamic algorithms are least problematic in computing ocean surface turbulent fluxes? *J. Climate*, **16,** 619–635.

Busalacchi, A. J., M. J. McPhaden, J. Picaut, and S. R. Springer, 1990: Sensitivity of wind-driven tropical Pacific Ocean simulations on seasonal and interannual time scales. *J. Mar. Syst.*, **1,** 119–154.

——, R. M. Atlas, and E. C. Hackert, 1993: Comparison of Special Sensor Microwave Imager vector wind stress with model-derived and subjective products for the tropical Pacific. *J. Geophys. Res.*, **98,** 6961–6977.

Cardone, V. J., J. G. Greenwood, and M. A. Cane, 1990: On trends in historical marine wind data. *J. Climate*, **3,** 113–127.

Cassou, C., and C. Perigaud, 2000: ENSO simulated with intermediate coupled models and evaluated with observations over 1970–1998. Part II: Role of the off-equatorial ocean and meridional winds. *J. Climate*, **13,** 1635–1663.

Chelton, D. B., and Coauthors, 2001: Observations of coupling between surface wind stress and sea surface temperature in the eastern tropical Pacific. *J. Climate*, **14,** 1479–1498.

Chen, D., 2003: A comparison of wind products in the context of ENSO prediction. *Geophys. Res. Lett.*, **30**, 1107, doi:10.1029/2002GL016121.

——, S. E. Zebiak, A. J. Busalacchi, and M. A. Cane, 1995: An improved procedure for El Niño forecasting: Implications for predictability. *Science*, **269,** 1699–1702.

——, M. A. Cane, and S. E. Zebiak, 1999: The impact of NSCAT winds on predicting the 1997/1998 El Niño: A case study with the Lamont-Doherty Earth Observatory model. *J. Geophys. Res.,* **104,** 11 321–11 327.

——, ——, ——, R. Canizares, and A. Kaplan, 2000: Bias correction of an ocean–atmosphere coupled model. *Geophys. Res. Lett.,* **27,** 2585–2588.

Chiang, J. C. H., S. E. Zebiak, and M. A. Cane, 2001: Relative roles of elevated heating and surface temperature gradients in driving anomalous surface winds over tropical oceans. *J. Atmos. Sci.,* **58,** 1371–1394.

Clarke, A. J., and A. Lebedev, 1996: Long-term changes in the equatorial Pacific trade winds. *J. Climate,* **9,** 1020–1029.

——, and ——, 1997: Interannual and decadal changes in equatorial wind stress in the Atlantic, Indian, and Pacific Oceans and the eastern ocean coastal response. *J. Climate,* **10,** 1722–1729.

da Silva, A. M., C. C. Young, and S. Levitus, 1994: *Algorithms and Procedures.* Vol. 1, *Atlas of Surface Marine Data 1994,* NOAA Atlas NESDIS 6, 83 pp.

Dewitte, B., and C. Perigaud, 1996: El Niño–La Niña events simulated with Cane and Zebiak's model and observed with satellite or in situ data. Part II: Model forced with observations. *J. Climate,* **9,** 1188–1207.

Fairall, C. W., E. F. Bradley, D. P. Rogers, J. B. Edson, and G. S. Young, 1996: Bulk parameterization of air–sea fluxes for Tropical Ocean Global Atmosphere Coupled Ocean–Atmosphere Response Experiment. *J. Geophys. Res.,* **101,** 3747–3764.

——, ——, J. E. Hare, A. A. Grachev, and J. B. Edson, 2003: Bulk parameterization of air–sea fluxes: Updates and verification for the COARE algorithm. *J. Climate,* **16,** 571–591.

Gaffen, D. J., T. P. Barnett, and W. P. Elliott, 1991: Space and time scales of global tropospheric moisture. *J. Climate,* **4,** 989–1008.

Garreaud, R. D., and D. S. Battisti, 1999: Interannual (ENSO) and interdecadal (ENSO-like) variability in the Southern Hemisphere tropospheric circulation. *J. Climate,* **12,** 2113–2123.

Gibson, J. K., P. Kållberg, S. Uppala, A. Hernandez, A. Nomura, and E. Serrano, 1999: ERA-15 description, Version 2. ECMWF Reanalysis Project Report Series 1, ECMWF Tech. Rep., Shinfield Park, Reading, United Kingdom, 84 pp.

Gordon, C., and R. A. Corry, 1991: A model simulation of the seasonal cycle in the tropical Pacific Ocean using climatological and modeled surface forcing. *J. Geophys. Res.,* **96,** 847–864.

Goswami, B. N., and M. A. Thomas, 2000: Coupled ocean–atmosphere inter-decadal modes in the Tropics. *J. Meteor. Soc. Japan,* **78,** 765–775.

Graham, N. E., 1994: Decadal-scale climate variability in the tropical and North Pacific during the 1970s and 1980s: Observations and model results. *Climate Dyn.,* **10,** 135–162.

Grima, N., A. Bentamy, K. Katsaros, Y. Quilfen, P. Delecluse, and C. Levy, 1999: Sensitivity of an oceanic general circulation model forced by satellite wind stress fields. *J. Geophys. Res.,* **104,** 7967–7989.

Gu, D., and S. G. H. Philander, 1995: Secular changes of annual and interannual variability in the Tropics during the past century. *J. Climate,* **8,** 864–876.

Hackert, E. C., A. J. Busalacchi, and R. Murtugudde, 2001: A wind comparison study using an ocean general circulation model for the 1997–1998 El Niño. *J. Geophys. Res.,* **106,** 2345–2362.

Harrison, D. E., and N. K. Larkin, 1998: ENSO sea surface temperature and wind anomalies, 1946–1993. *Rev. Geophys.,* **36,** 353–399.

——, W. S. Kessler, and B. S. Giese, 1989: Ocean circulation model hindcasts of the 1982–83 El Niño: Thermal variability along the ship-of-opportunity tracks. *J. Phys. Oceanogr.,* **19,** 397–418.

Harrison, M. J., A. Rosati, B. J. Soden, E. Galanti, and E. Tziperman, 2002: An evaluation of air–sea flux products for ENSO simulation and prediction. *Mon. Wea. Rev.,* **130,** 723–732.

Hashizume, H., S.-P. Xie, M. Fujiwara, M. Shiotani, T. Watanabe, Y. Tanimoto, W. T. Liu, and K. Takeuchi, 2002: Direct observations of atmospheric boundary layer response to SST variations associated with tropical instability waves over the eastern equatorial Pacific. *J. Climate,* **15,** 3379–3393.

Hayes, S. P., M. J. McPhaden, and J. M. Wallace, 1989: The influence of sea surface temperature on surface wind in the eastern equatorial Pacific: Weekly to monthly variability. *J. Climate,* **2,** 1500–1506.

Huang, B., 2001: The response of a global ocean general circulation model to surface wind stress forcing from NCEP reanalysis for 1950–1998. *Proc. WCRP/SCOR Workshop on Intercomparison and Validation of Ocean–Atmosphere Flux Fields,* Bolger Center, Potomac, MD, WCRP-115, WMO/TD WCRP/SCOR/1083.

IFREMER/CERSAT, 2002: QuikSCAT scatterometer mean wind field products user manual. C2-MUT-W-04-IF, version 1.0, IFREMER/CERSAT, Plouzane, France, 47 pp.

Isemer, H. J., and L. Hasse, 1991: The scientific Beaufort equivalent scale: Effects on wind statistics and climatological air–sea flux estimates in the North Atlantic Ocean. *J. Climate,* **4,** 819–836.

Janowiak, J. E., A. Gruber, C. R. Kondragunta, R. E. Livezey, and G. J. Huffman, 1998: A comparison of the NCEP–NCAR reanalysis precipitation and the GPCP rain gauge–satellite combined dataset with observational error considerations. *J. Climate,* **11,** 2960–2979.

Ji, M., D. W. Behringer, and A. Leetmaa, 1998: An improved coupled model for ENSO prediction and implications for ocean initialization. Part II: The coupled model. *Mon. Wea. Rev.,* **126,** 1022–1034.

Jones, I. S. F., and Y. Toba, Eds., 2001: *Wind Stress Over the Ocean.* Cambridge University Press, 306 pp.

Josey, S. A., E. C. Kent, and P. K. Taylor, 2002: Wind stress forcing of the ocean in the SOC climatology: Comparisons with the NCEP–NCAR, ECMWF, UWM/COADS, and Hellerman and Rosenstein datasets. *J. Phys. Oceanogr.,* **32,** 1993–2019.

Kachi, M., and T. Nitta, 1997: Decadal variations of the global atmosphere–ocean system. *J. Meteor. Soc. Japan,* **75,** 657–675.

Kalnay, E., M. Kanamitsu, R. Kistler, and Coauthors, 1996: The NCEP/NCAR 40-Year Reanalysis Project. *Bull. Amer. Meteor. Soc.,* **77,** 437–471.

Kang, I.-S., and J.-S. Kug, 2002: El Niño and La Niña sea surface temperature anomalies: Asymmetry characteristics associated with their wind stress anomalies. *J. Geophys. Res.,* **107**, 4372, doi:10.1029/2001JD000393.

Kelly, K. A., S. Dickinson, and Z. Yu, 1999: NSCAT tropical wind stress maps: Implications for improving ocean modeling. *J. Geophys. Res.,* **104,** 11 291–11 310.

——, ——, M. J. McPhaden, and G. C. Johnson, 2001: Ocean currents evident in satellite wind data. *Geophys. Res. Lett.,* **28,** 2469–2472.

Kent, E. C., and P. K. Taylor, 1997: Choice of a Beaufort equivalent scale. *J. Atmos. Oceanic Technol.,* **14,** 228–242.

——, P. G. Challenor, and P. K. Taylor, 1999: A statistical determination of the random observational errors present in voluntary observing ships meteorological reports. *J. Atmos. Oceanic Technol.,* **16,** 905–914.

Kessler, W. S., 2002: Is ENSO a cycle or a series of events? *Geophys. Res. Lett.,* **29**, 2125, doi:10.1029/2002GL015924.

Kirtman, B. P., 1997: Oceanic Rossby wave dynamics and the ENSO period in a coupled model. *J. Climate,* **10,** 1690–1704.

——, and E. K. Schneider, 1996: Model-based estimates of equatorial Pacific wind stress. *J. Climate,* **9,** 1077–1091.

——, Y. Fan, and E. K. Schneider, 2002: The COLA global coupled and anomaly coupled ocean–atmosphere GCM. *J. Climate,* **15,** 2301–2320.

Kistler, R., and Coauthors, 2001: The NCEP–NCAR 50-year reanalysis: Monthly means CD-ROM and documentation. *Bull. Amer. Meteor. Soc.,* **82,** 247–268.

Kleeman, R., 1991: A simple model of the atmospheric response to ENSO sea surface temperature anomalies. *J. Atmos. Sci.,* **48,** 3–18.

——, G. Wang, and S. Jewson, 2001: Surface flux response to in-

terannual tropical Pacific sea surface temperature variability in AMIP models. *Climate Dyn.,* **17,** 627–641.
Krishnamurthy, V., and B. N. Goswami, 2000: Indian monsoon–ENSO relationship on interdecadal timescale. *J. Climate,* **13,** 579–595.
Kug, J.-S., I.-S. Kang, and S. E. Zebiak, 2001: The impacts of the model assimilated wind stress data in the initialization of an intermediate ocean and the ENSO predictability. *Geophys. Res. Lett.,* **28,** 3713–3716.
Landsteiner, M. C., M. J. McPhaden, and J. Picaut, 1990: On the sensitivity of Sverdrup transport estimates to the specification of wind stress forcing in the tropical Pacific. *J. Geophys. Res.,* **95,** 1681–1691.
Larkin, N. K., and D. E. Harrison, 2002: ENSO warm (El Niño) and cold (La Niña) event life cycles: Ocean surface anomaly patterns, their symmetries, asymmetries, and implications. *J. Climate,* **15,** 1118–1140.
Latif, M., 1987: Tropical ocean circulation experiments. *J. Phys. Oceanogr.,* **17,** 246–263.
——, R. Kleeman, and C. Eckert, 1997: Greenhouse warming, decadal variability, or El Niño? An attempt to understand the anomalous 1990s. *J. Climate,* **10,** 2221–2239.
Lau, K.-M., and H. Weng, 1995: Climate signal detection using wavelet transform: How to make a time series sing. *Bull. Amer. Meteor. Soc.,* **76,** 2391–2402.
Lindzen, R. S., and S. Nigam, 1987: On the role of sea surface temperature gradients in forcing low-level winds and convergence in the Tropics. *J. Atmos. Sci.,* **44,** 2418–2436.
Liu, W. T., W. Tang, and R. Atlas, 1993: Sea surface temperature exhibited by an ocean general circulation model in response to wind forcing derived from satellite data. *Remote Sensing of the Oceanic Environment,* I. S. F. Jones, Y. Sugimori, and R. W. Stewart, Eds., Seibutsu Kenkyusha, 350–355.
——, X. Xie, P. S. Polito, S.-P. Xie, and H. Hashizume, 2000: Atmospheric manifestation of tropical instability wave observed by QuikSCAT and Tropical Rain Measuring Mission. *Geophys. Res. Lett.,* **27,** 2545–2548.
McPhaden, M. J., A. J. Busalacchi, and J. Picaut, 1988: Observations and wind-forced model simulations of the mean seasonal cycle in tropical Pacific sea surface topography. *J. Geophys. Res.,* **93,** 8131–8146.
Meissner, T., D. Smith, and F. Wentz, 2001: A 10 year intercomparison between collocated Special Sensor Microwave Imager oceanic surface wind speed retrievals and global analyses. *J. Geophys. Res.,* **106,** 11 731–11 742.
Milliff, R. F., W. G. Large, J. Morzel, G. Danabasoglu, and T. M. Chin, 1999: Ocean general circulation model sensitivity to forcing from scatterometer winds. *J. Geophys. Res.,* **104,** 11 337–11 358.
Moore, A. M., J. Vialard, A. T. Weaver, D. L. T. Anderson, R. Kleeman, and J. R. Johnson, 2003: The role of air–sea interaction in controlling the optimal perturbations of low-frequency tropical coupled ocean–atmosphere modes. *J. Climate,* **16,** 951–968.
Morrissey, M. L., 1990: An evaluation of ship data in the equatorial western Pacific. *J. Climate,* **3,** 99–112.
——, and N. E. Graham, 1996: Recent trends in rain gauge precipitation measurements from the tropical Pacific: Evidence for an enhanced hydrologic cycle. *Bull. Amer. Meteor. Soc.,* **77,** 1207–1219.
Neelin, J. D., 1990: A hybrid coupled general circulation model for El Niño studies. *J. Atmos. Sci.,* **47,** 674–693.
Nitta, T., and S. Yamada, 1989: Recent warming of tropical sea surface temperature and its relationship to the Northern Hemisphere circulation. *J. Meteor. Soc. Japan,* **67,** 375–383.
——, and M. Kachi, 1994: Interdecadal variations of precipitation over the tropical Pacific and Indian Oceans. *J. Meteor. Soc. Japan,* **72,** 823–831.
Patoux, J., R. C. Foster, and R. A. Brown, 2003: Global pressure fields from scatterometer winds. *J. Appl. Meteor.,* **42,** 813–826.
Pegion, P. J., M. A. Bourassa, D. M. Legler, and J. J. O'Brien, 2000: Objectively derived daily ''winds'' from satellite scatterometer data. *Mon. Wea. Rev.,* **128,** 3150–3168.
Putman, W. M., D. M. Legler, and J. J. O'Brien, 2000: Interannual variability of synthesized FSU and NCEP–NCAR reanalysis pseudostress products over the Pacific Ocean. *J. Climate,* **13,** 3003–3016.
Quilfen, Y., B. Chapron, and D. Vandemark, 2001: The ERS scatterometer wind measurement accuracy: Evidence of seasonal and regional biases. *J. Atmos. Oceanic Technol.,* **18,** 1684–1697.
Reynolds, R. W., K. Arpe, C. Gordon, S. P. Hayes, A. Leetmaa, and M. J. McPhaden, 1989: A comparison of tropical Pacific surface wind analyses. *J. Climate,* **2,** 105–111.
Rienecker, M. M., R. A. Atlas, S. D. Schubert, and C. S. Willett, 1996: A comparison of surface wind products over the North Pacific Ocean. *J. Geophys. Res.,* **101,** 1011–1023.
Saji, N. H., and B. N. Goswami, 1997: Intercomparison of the seasonal cycle of tropical surface stress in 17 AMIP atmospheric general circulation models. *Climate Dyn.,* **13,** 561–585.
Santer, B. D., J. J. Hnilo, T. M. L. Wigley, J. S. Boyle, C. Doutriaux, M. Fiorino, D. E. Parker, and K. E. Taylor, 1999: Uncertainties in ''observational'' estimates of temperature change in the free atmosphere. *J. Geophys. Res.,* **104,** 6305–6333.
Shinoda, T., H. H. Hendon, and J. Glick, 1999: Intraseasonal surface fluxes in the tropical western Pacific and Indian Oceans from NCEP reanalyses. *Mon. Wea. Rev.,* **127,** 678–693.
Simmons, A. J., and J. K. Gibson, 2000: The ERA-40 Project Plan. ERA-40 Project Report Series No. 1, ECMWF Tech. Rep., Shinfield Park, Reading, United Kingdom, 63 pp.
Smith, S. D., 1988: Coefficients for sea surface wind stress, heat flux, and wind profiles as a function of wind speed and temperature. *J. Geophys. Res.,* **93,** 15 467–15 472.
——, D. M. Legler, and K. V. Verzone, 2001: Quantifying uncertainties in NCEP reanalyses using high-quality research vessel observations. *J. Climate,* **14,** 4062–4072.
Smith, T. M., R. W. Reynolds, R. E. Livezey, and D. C. Stokes, 1996: Reconstruction of historical sea surface temperatures using empirical orthogonal functions. *J. Climate,* **9,** 1403–1420.
Stammer, D., and Coauthors, 2002: Global ocean circulation during 1992–1997, estimated from ocean observations and a general circulation model. *J. Geophys. Res.,* **107**, 3118, doi:10.1029/2001JC000888.
Sterl, A., 2001: On the impact of gap-filling algorithms on variability patterns of reconstructed oceanic surface fields. *Geophys. Res. Lett.,* **28,** 2473–2476.
Stevens, B., J. Duan, J. C. McWilliams, M. Munnich, and J. D. Neelin, 2002: Entrainment, Rayleigh friction, and boundary layer winds over the tropical Pacific. *J. Climate,* **15,** 30–44.
Stricherz, J. N., D. M. Legler, and J. J. O'Brien, 1997: Tropical Pacific Ocean. Vol. II, TOGA Pseudostress Atlas 1985–1994. COAPS Tech. Rep. 97-2, COAPS/The Florida State University, Tallahassee, FL.
Tang, Y., 2002: Hybrid coupled models of the tropical Pacific: I. Interannual variability. *Climate Dyn.,* **19,** 331–342.
Taylor, P. K., 2001: Intercomparison and validation of ocean–atmosphere energy flux fields. Joint WCRP/SCOR Working Group on Air–Sea Fluxes Final Report, WMO/TD 1036, WCRP-112, Geneva, Switzerland, 308 pp.
——, E. C. Kent, M. J. Yelland, and B. I. Moat, 1999: The accuracy of marine surface winds from ships and buoys. *Proc. WMO Workshop on Advances in Marine Climatology,* Vancouver, BC, Canada, World Meteorological Organization, 59–68.
Torrence, C., and P. J. Webster, 1998: The annual cycle of persistence in the El Niño/Southern Oscillation. *Quart. J. Roy. Meteor. Soc.,* **124,** 1985–2004.
——, and G. P. Compo, 1999: A practical guide to wavelet analysis. *Bull. Amer. Meteor. Soc.,* **79,** 61–78.
——, and P. J. Webster, 1999: Interdecadal changes in the ENSO–monsoon system. *J. Climate,* **12,** 2679–2690.
Trenberth, K. E., 1990: Recent observed interdecadal climate changes

in the Northern Hemisphere. *Bull. Amer. Meteor. Soc.,* **71,** 988–993.
——, and J. W. Hurrell, 1994: Decadal atmosphere–ocean variations in the Pacific. *Climate Dyn.,* **9,** 303–319.
——, W. G. Large, and J. G. Olson, 1990: The mean annual cycle in global ocean wind stress. *J. Phys. Oceanogr.,* **20,** 1742–1760.
——, D. P. Stepaniak, J. W. Hurrell, and M. Fiorino, 2001: Quality of reanalyses in the Tropics. *J. Climate,* **14,** 1499–1510.
Wallace, J. M., T. P. Mitchell, and C. Deser, 1989: The influence of sea-surface temperature on surface wind in the eastern equatorial Pacific: Seasonal and interannual variability. *J. Climate,* **2,** 1492–1499.
Wang, B., 1995: Interdecadal changes in El Niño onset in the last four decades. *J. Climate,* **8,** 267–285.
——, and T. Li, 1993: A simple tropical atmosphere model of relevance to short-term climate variations. *J. Atmos. Sci.,* **50,** 260–284.
——, and Y. Wang, 1996: Temporal structure of the Southern Oscillation as revealed by waveform and wavelet analysis. *J. Climate,* **9,** 1586–1598.
——, and S.-I. An, 2002: A mechanism for decadal changes of ENSO behavior: Roles of background wind changes. *Climate Dyn.,* **18,** 475–486.
Ward, N. M., 1992: Provisionally corrected surface wind data, worldwide ocean-atmosphere surface fields, and Sahelian rainfall variability. *J. Climate,* **5,** 454–475.
——, and B. J. Hoskins, 1996: Near-surface wind over the global ocean 1949–1988. *J. Climate,* **9,** 1877–1895.
Wittenberg, A. T., 2002: ENSO response to altered climates. Ph.D. thesis, Princeton University, 475 pp.
Wright, D. G., and K. R. Thompson, 1983: Time-averaged forms of the nonlinear stress law. *J. Phys. Oceanogr.,* **13,** 341–345.
Wu, R., and S.-P. Xie, 2003: On equatorial Pacific surface wind changes around 1977: NCEP–NCAR reanalysis versus COADS observations. *J. Climate,* **16,** 167–173.
Xie, S.-P., T. Kunitani, A. Kubokawa, M. Nonaka, and S. Hosoda, 2000: Interdecadal thermocline variability in the North Pacific for 1958–97: A GCM simulation. *J. Phys. Oceanogr.,* **30,** 2798–2813.
Yang, F., A. Kumar, and W. Wang, 2001: Seasonal dependence of surface wind stress variability on SST and precipitation over the tropical Pacific. *Geophys. Res. Lett.,* **28,** 3171–3174.
Yang, Y. J., T. Y. Tang, and R. H. Weisberg, 1997: Basin-wide zonal wind stress and ocean thermal variations in the equatorial Pacific Ocean. *J. Geophys. Res.,* **102,** 911–927.
Yelland, M. J., B. I. Moat, P. K. Taylor, R. W. Pascal, J. Hutchings, and V. C. Cornell, 1998: Wind stress measurements from the open ocean corrected for airflow distortion by the ship. *J. Phys. Oceanogr.,* **28,** 1511–1526.
Yu, Z., and D. W. Moore, 2000: Validating the NSCAT winds in the vicinity of the Pacific Intertropical Convergence Zone. *Geophys. Res. Lett.,* **27,** 2121–2124.
Zebiak, S. E., 1990: Diagnostic studies of Pacific surface winds. *J. Climate,* **3,** 1016–1031.
Zhang, C., and J. Gottschalck, 2002: SST anomalies of ENSO and the Madden–Julian oscillation in the equatorial Pacific. *J. Climate,* **15,** 2429–2445.
——, H. H. Hendon, W. S. Kessler, and A. J. Rosati, 2001: A workshop on the MJO and ENSO. *Bull. Amer. Meteor. Soc.,* **82,** 971–976.
Zhang, Y., J. M. Wallace, and D. S. Battisti, 1997: ENSO-like interdecadal variability: 1900–93. *J. Climate* **10,** 1004–1020.